

Article

Influence of Boron on Initial Austenite Grain Size and Hot Deformation Behavior of Boron Microalloyed Steels

Yong-liang Gao, Xiang-xin Xue * and He Yang

Liaoning Key Laboratories of Ecological Utilization Technology of Boron Resources and Boron Materials, Northeastern University, Shenyang 110819, China; E-Mails: gufeng220630@163.com (Y.G.); yangh@smm.neu.edu.cn (H.Y.)

* Author to whom correspondence should be addressed; E-Mail: xuexx@mail.neu.edu.cn; Tel.: +86-24-8368-1711.

Academic Editors: Umit B. Demirci, Philippe Miele and Pascal G. Yot

Received: 11 October 2015 / Accepted: 16 November 2015 / Published: 24 November 2015

Abstract: The initial austenite grain size of boron microalloyed steel with three different amounts of boron (20, 40, and 60 ppm) was investigated under different heating temperatures (1150, 1100, and 1050 °C), and hot compression tests of samples in a wide range of temperature (900–1100 °C) and strain rate (0.1–10 s⁻¹) were conducted. It was found that the initial austenite grain size increases with increasing temperature and boron content. The flow stress decreased with increasing boron content at lower strain rates. The flow stress constitutive equation of hot deformation was developed for the experimental steels; results showed that boron addition has the trend to reduce the hot deformation activation energy. The characteristic points of the flow curves were analyzed. Results revealed that the peak and critical stress decreased in response to an increase of boron content. The work-hardening behavior of both steels was investigated, and it was found that boron addition can decrease the work-hardening rate when strained at lower strain rates. On the contrary, peak and critical strains increased as boron content increased, indicating that boron has the ability to delay the onset of dynamic recrystallization.

Keywords: boron-tread steels; initial austenite grain; hot deformation; constitutive equation; dynamic recrystallization

1. Introduction

High strength low alloy steels (HSLA) are attracting a strong interest from various industrial sectors, particularly in the automotive industry [1,2]. This is due to their exceptional strength and ductility as compared to other conventional grades of steel. The mechanical properties of HSLA steel depend on its grain size, its volume fraction martensite or bainite and the carbon content of each phase. The ferrite grain refinement of steels has attracted considerable interest from investigators due to its unique role of increasing both strength and toughness [3]. It is well known that the refinement of the initial austenite grain size and thermo-mechanical processing (TMP) are the most common method to refine the microstructural for hot-rolled steel. Furthermore, various phenomena have been shown to occur during the high temperature deformation process of austenitic steel: (1) work hardening (WH), (2) dynamic recovery (DRV) and (3) dynamic recrystallization (DRX) depending on tunable process conditions such as deformation temperature and strain rate. DRX plays a major role in reducing the flow stress and the grain size [3]. Therefore, it is necessary that the influence of alloying elements on initial austenite grain size and hot deformation behavior is well understood.

Boron is known to be an effective alloying element used to increase the hardenability of HSLA. Generally speaking, hardenability occurs because boron atoms easily segregate to prior austenite grain boundaries, lowering the grain boundary energy while retarding the transformation of austenite to ferrite [4–6]. Advantageously, the grain boundary segregation of boron in steel occurs via two mechanisms: (1) equilibrium and (2) non-equilibrium segregation. Qualitatively, non-equilibrium segregation proves to be the dominant contributing factor in conventional heat treatment conditions of steel [7]. Migration of boron to the austenite grain boundaries affects the thermodynamics of the respective boundaries. It can effect the austenite grain and hot deformation behavior. Although many investigations have reported the effect of boron on hot stamped [8], hot ductility [9], phase transformation [10], hardenability [11] and boundary segregation behavior [12], systematic work of boron content on initial austenite grain size and hot deformation behavior is lacking. Mun [11] only concluded that the hardenability of the boron-bearing steel decreases with increasing austenite grain size, but the effect of boron content on initial austenite grain size was not clarified in this study. In addition, the effect of boron on hot flow behavior is still disputed by numerous authors. Mejía [13,14] and López-Chipres [15] have reported that boron addition generates a softening effect and accelerates the onset of DRX. On the other hand, Kim [16], Banks [17] and Stumpf [18] observed that boron had a delayed effect of the onset of DRX. However, in these studies [13–18], the effect of boron content on initial austenite grain size and activation energy for hot deformation was not discussed. Therefore, there is an obvious scientific and commercial significance for more insight into influence of boron content on initial austenite grain size and hot deformation behavior.

In the present paper, the initial austenite grain size of steels with different boron content was investigated under different heating temperatures. In addition, the activation energy and constitutive equation for experimental steels were given. Moreover, the flow curves at different deformation and critical parameters as a function of boron composition are presented.

2. Results and Discussion

2.1. Influence of Boron Content on Initial Austenite Grain

Figure 1 shows the morphology of initial austenite grains of steels B1, B2 and B3 under various heating conditions respectively. Figure 2 shows the relationship between temperatures and average austenite grain sizes for steels B1, B2 and B3. It can be seen that the initial austenite grain size in all the regions increases with an increase in austenitization temperature. In addition, the austenite grain size of steel with higher boron content is larger than steel with lower boron content at each temperature.

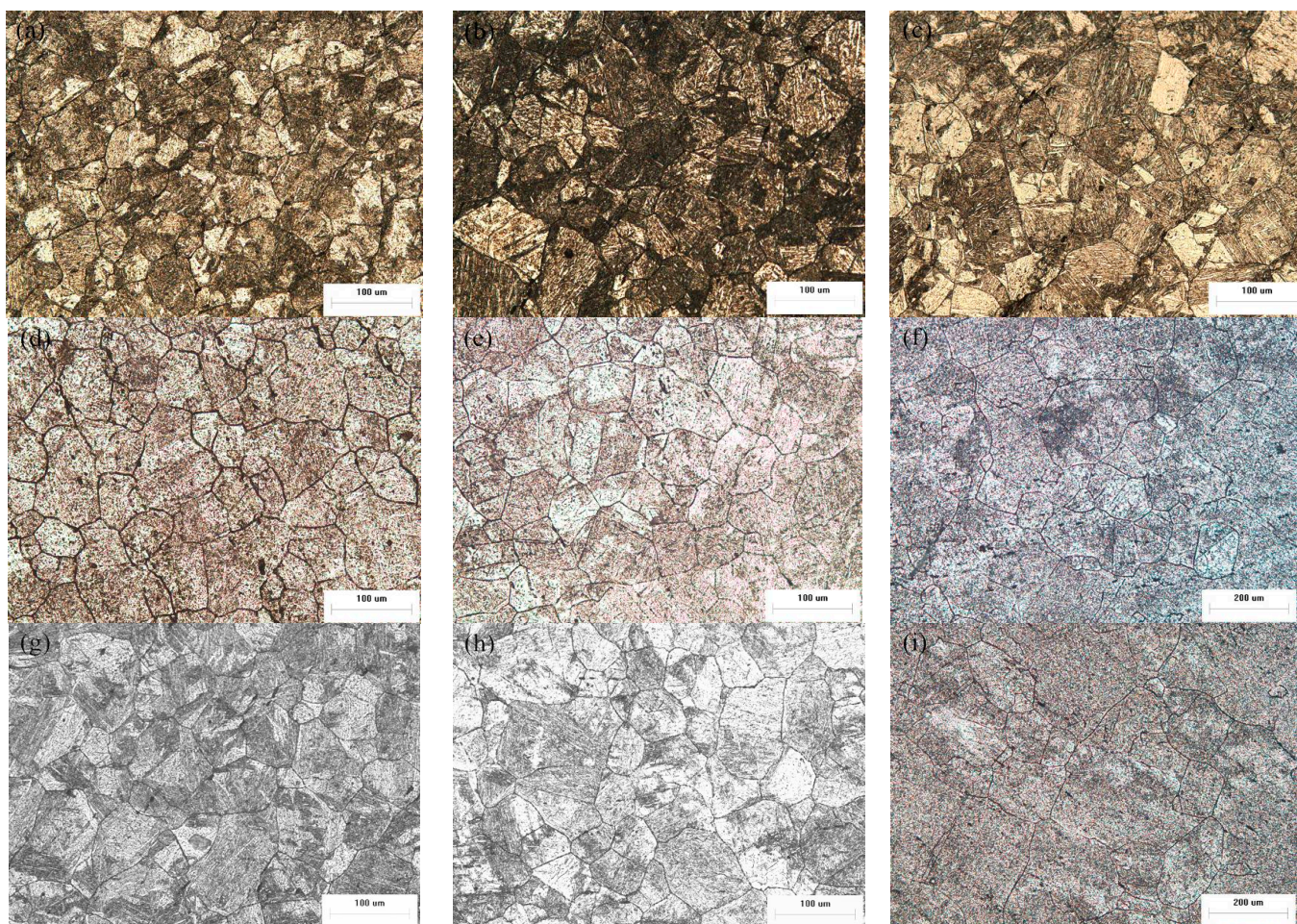


Figure 1. Optical micrographs of initial austenite grain at different austenitizing temperatures: (a) B1, 1050 °C; (b) B1, 1100 °C; (c) B1, 1150 °C; (d) B2, 1050 °C; (e) B2, 1100 °C; (f) B2, 1150 °C; (g) B3, 1050 °C; (h) B3, 1100 °C; (i) B3, 1150 °C.

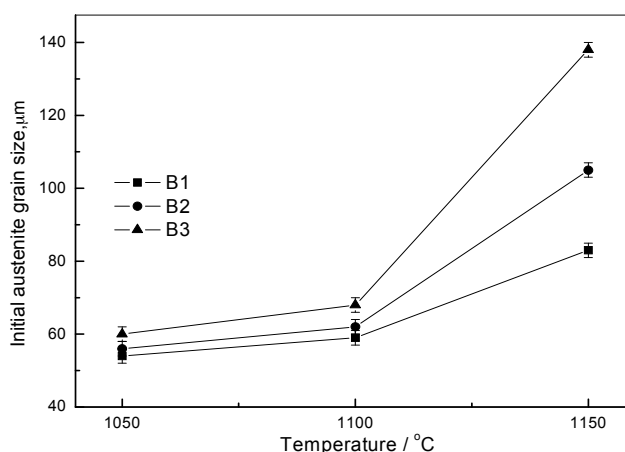


Figure 2. Initial austenite grain size of specimens at different austenitizing temperatures.

The initial austenite grain size of both steels is shown in Table 1. It can be seen that the grain size of steel B1 increases from 54 to 83 μm , while that of steel B2 and B3 increase from 56 to 105 μm and from 60 to 138 μm , respectively. This result indicates that additional boron can coarsen initial austenite grain size. This trend can be attributed to the fact that the amount of fine AlN reduces because of the formation of BN. It has been reported that AlN can pin the austenite grain boundaries and retard the growth of austenite grain [19]. Figure 3 shows that BN can be produced earlier than AlN at an identical temperature [20]. Figure 4 shows the characteristics and compositions of precipitates in steel B3. EDS analysis indicates that the particles in steel B3 contain B and N elements. Consequently, it indicates that the content of AlN reduces because of the formation of BN. Li [21] also observed a different content of AlN present in boron-free and boron-treated steel, with expected results showing that the amount of AlN decreases in boron-treated steel. In Bao's work [22], the results showed that when the size of BN particles is about 10 nm, they are spherical and distributed along grain boundaries. When BN particles are larger than 20 nm, they are rod-like and distributed along grain boundaries. It can be seen that the size of BN is much larger. In addition, Chown [23] found that boron has a tendency to segregate to high-angle grain boundaries and to interfaces of incoherent particles such as MnS and Al_2O_3 . This leads to the formation of complex precipitates, such as $[\text{MnS} + \text{BN}]$, in which a spherical MnS precipitate is surrounded by polycrystalline aggregates of hexagonal BN. This coarsened the boron-containing precipitates. The size of AlN precipitates is much smaller than BN precipitates. The content of AlN reduces via boron addition. Consequently, additional boron can coarsen initial austenite grain size.

Table 1. Initial austenite grain size of the test steels (μm).

Steels	1050 °C	1100 °C	1150 °C
B1	54	59	83
B2	56	62	105
B3	60	68	138

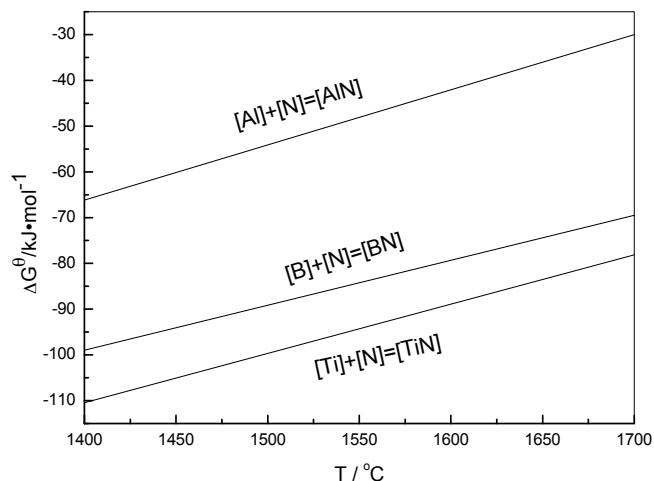


Figure 3. The ΔG^θ of producing AlN, BN, and TiN at different temperatures.

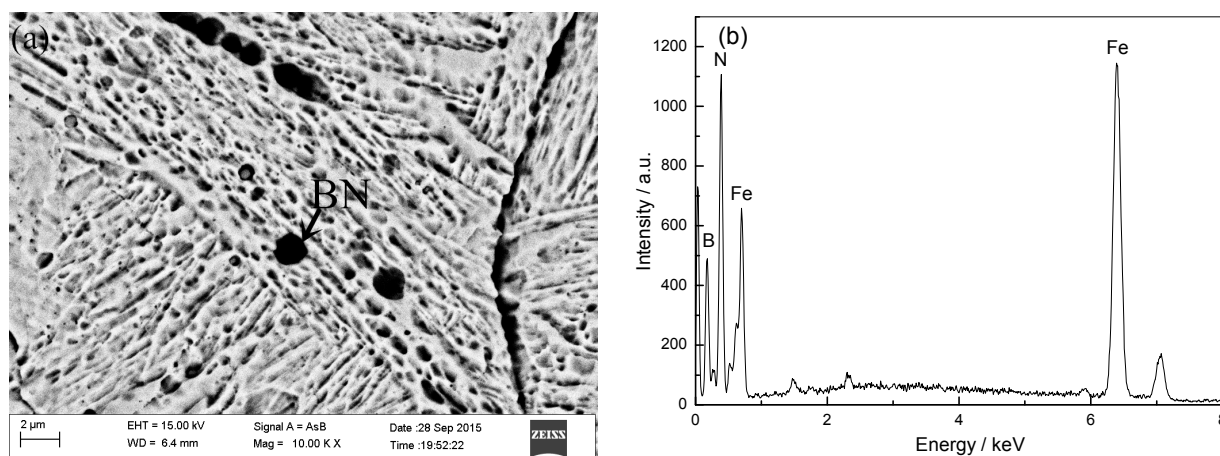


Figure 4. SEM morphology of BN precipitate (a) and EDS spectrum; (b) in steel B3.

2.2. Influence of Boron Content on Hot Deformation Behavior

2.2.1. Flow Stress Curves

The flow stress curves of boron-treated steels deformed at distinct temperatures and strain rates are shown in Figure 5. It can be seen that the deformation temperatures and strain rates have considerable influence on the hot deformation behavior of the samples. The flow stress of each steel decreases significantly as temperature increases and strain rate decreases. Furthermore, the stress–strain curves (Figure 5) demonstrate a distinct classification of mechanisms taking place, DRV and DRX. Generally, stress rises to a peak and softens toward a steady state region, revealing the occurrence of DRX, and flow curves without well-defined peak stresses are generally believed to display DRV as the only restoring mechanism. DRV occurs for all deformation temperatures at a strain rate of 10 s^{-1} . When the strain rate decreases to 1 s^{-1} , DRV is only observed to occur at a deformation temperature of $900 \text{ }^\circ\text{C}$. DRX occurs for all deformation temperatures at a strain rate of 0.1 s^{-1} .

From Figure 5a,b, it can also be seen that the DRX plots demonstrate that steel containing a higher boron concentration yields a lower peak stress value when compared to a sample with less boron at an identical temperature and strain rate. Accordingly, it is believed that boron has a solid

solution-softening effect when DRX occurs. In the DRV process, Figure 5c displays B2 samples possessing an increased flow resistance in relation to the B3 samples, which only show a higher flow resistance relative to B1 samples at high strain rate (10 s^{-1}). The expressed data proves to be identical with Kim's [16] research. The reasoning for this phenomenon is that boron atoms have insufficient time for reorganization, precluding them from having any significant effect on softening under high strain rate. Additionally, the results exhibit that boron atoms hinder dislocation motion at high strain rates, and pinning effect decreases when boron reaches a distinct concentration limit.

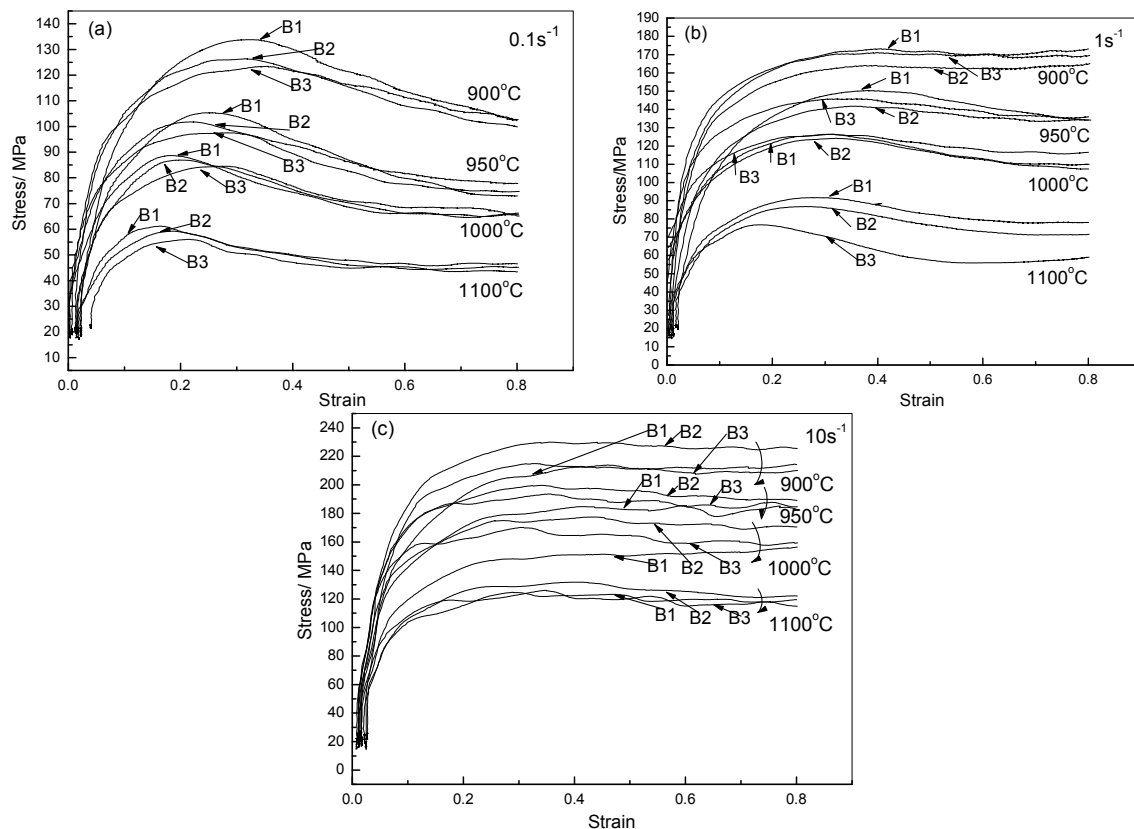


Figure 5. Flow curves for different steels at different temperatures and strain rates.

2.2.2. Constitutive Analysis

To investigate the effect of boron on the hot deformation behaviors, it is necessary to study the activation energy for deformation. Usually, the effects of the temperatures and strain rates on the deformation behaviors can be represented by Zener-Hollomon parameter, Z , in an exponent-type equation. Arrhenius equations are often employed to study the influence of temperature and strain rate on flow stress, and the hyperbolic law in the Arrhenius equation gives better approximations between Z parameter and stress [24]:

$$Z = \dot{\epsilon} \exp(Q/RT) \quad (1)$$

$$\dot{\epsilon} = A [\sinh(\alpha\sigma)]^n \exp(-Q/RT) \text{ for all } \sigma \quad (2)$$

where

$$[\sinh(\alpha\sigma)]^n = \begin{cases} \sigma^{n_1} \rightarrow \alpha\sigma < 0.8 \\ \exp(\beta\sigma) \rightarrow \alpha\sigma > 1.2 \end{cases} \quad (3)$$

in which, $\dot{\epsilon}$ is the strain rate (s^{-1}), R is the universal gas constant ($8.31 \text{ J}\cdot\text{mol}^{-1}\cdot\text{K}^{-1}$), T is the absolute temperature (K), Q is the activation energy of hot deformation (kJ/mol), A , α , β , n_1 and n are the material constants, and σ is the flow stress (MPa). Characteristic stresses such as peak stress, steady state stress, or stress corresponding to a specific strain can be used in these equations [25]. The constitutive equations of the three steels are established using peak stress. The value of α can be calculated from $\alpha = \beta/n_1$.

For low ($\alpha\sigma_p < 0.8$) and high ($\alpha\sigma_p > 1.2$) stress levels, taking natural logarithms on both side of Equation (2) produces:

$$\ln\dot{\epsilon} = \ln A + n_1 \ln\sigma - (Q/RT) \quad (4)$$

$$\ln\dot{\epsilon} = \ln A + \beta\sigma - (Q/RT) \quad (5)$$

There is a linear relationship between $\ln\sigma_p$ and $\ln\dot{\epsilon}$ as well as between σ_p and $\ln\dot{\epsilon}$ at different deformation conditions, as shown in Figure 6a,b, respectively. The mean value of n_1 and β at different temperature can be computed as 6.7717 and 0.0607, so $\alpha = 0.0090$ for steel B1.

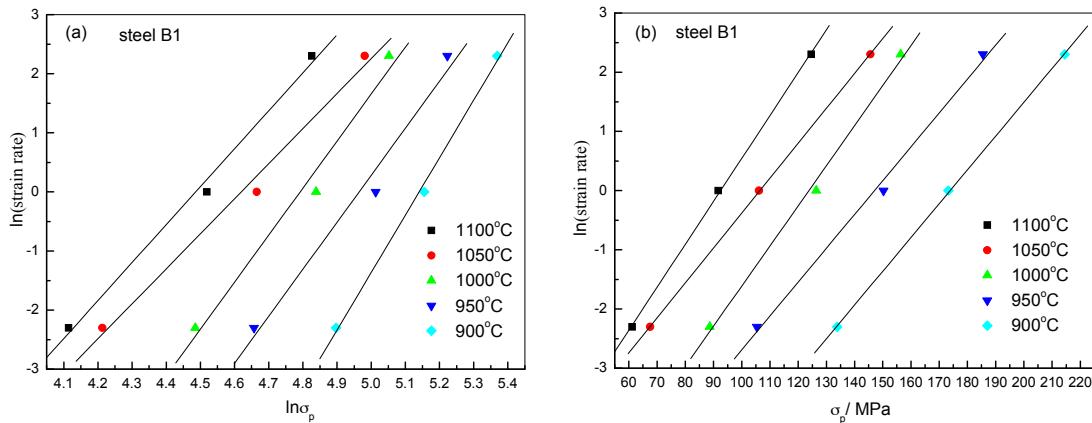


Figure 6. Relationship between $\ln(\text{strain rate})$ and (a) $\ln\sigma_p$; (b) σ_p .

Taking natural logarithms on both sides of Equations (2) and (6) can be obtained.

$$\ln\dot{\epsilon} = n \ln[\sinh(\alpha\sigma_p)] + \ln A - Q/(RT) \quad (6)$$

When T is constant, the partial differentiation of Equation (6) yields Equation (7).

$$n = \frac{\partial \ln \dot{\epsilon}}{\partial \ln[\sinh(\alpha\sigma_p)]} \quad (7)$$

In accordance with the relationship curves of $\ln\dot{\epsilon}$ and $\ln[\sinh(\alpha\sigma_p)]$ (Figure 7a), the average value of n can be estimated to be 5.4195 for steel B1.

When $\dot{\epsilon}$ is constant, the partial differentiation of Equation (6) yields Equation (8).

$$Q = Rn \frac{\partial \ln[\sinh(\alpha\sigma_p)]}{\partial (1/T)} \quad (8)$$

Figure 7b shows the relationship between $\ln[\sinh(\alpha\sigma_p)]$ and T^{-1} , which is a set of parallel lines. This means that the activation energy for hot deformation is the same, irrespective of the strain rate. Thus, the activation energy for steel B1 can be calculated according to Equation (8); it is 316.86 kJ/mol.

According to Equations (1) and (2), the following equation can be obtained.

$$Z = A[\sinh(\alpha\sigma_p)]^n \tag{9}$$

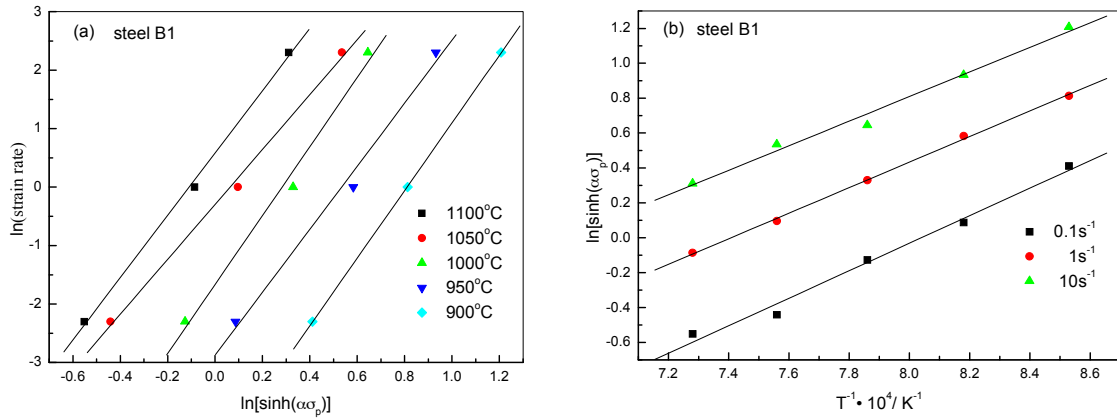


Figure 7. Relationship between $\ln[\sinh(\alpha\sigma_p)]$ and (a) $\ln(\text{strain rate})$; (b) T^{-1} .

The relationship between $[\sinh(\alpha\sigma_p)]^n$ and Z is presented in Figure 8, from which A can be readily computed as 1.501×10^{12} . The parameters in constitutive equations of all tested steels are shown in Table 2, and the constitutive equations of the experimental steels are shown as follows:

$$Z_{(B1)} = 1.501 \times 10^{12} [\sinh(0.0090\sigma_p)]^{5.4195} \tag{10}$$

$$Z_{(B2)} = 4.495 \times 10^{11} [\sinh(0.0078\sigma_p)]^{4.8760} \tag{11}$$

$$Z_{(B3)} = 6.009 \times 10^{10} [\sinh(0.0089\sigma_p)]^{4.6014} \tag{12}$$

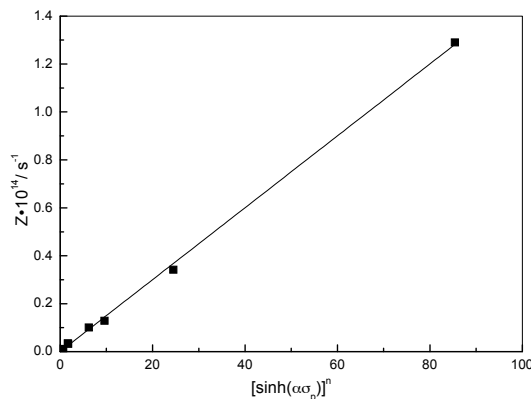


Figure 8. Relationship between $[\sinh(\alpha\sigma_p)]^n$ and Z .

Table 2. The parameters in the hot deformation constitutive equations.

Steels	β	n_1	α	n	Q (kJ/mol)	A
B1	0.0607	6.7717	0.0090	5.4195	316.86	1.501×10^{12}
B2	0.0465	6.0033	0.0078	4.8760	286.45	4.495×10^{11}
B3	0.0506	5.6940	0.0089	4.6014	277.91	6.009×10^{10}

Table 2 shows that the activation energy of steel B1 (316.86 kJ/mol) is higher than that of steel B2 (286.45 kJ/mol) and steel B3 (277.91 kJ/mol), which indicates that boron addition reduces the activation energy of steels in hot deformation. From Figure 9, it is seen that the Q value at different strains is also consistent with this trend: Steel B1 has the highest value, and steel B2 has a higher value than steel B3. These obtained results are in agreement with the results of other experiments [16]. On the basis of Jahazi's work [26], boron has dual nature in the austenite lattice, *i.e.*, boron atoms can occupy either substitutional or interstitial sites. He also found that a boron atom can make the transition from its substitutional position to an interstitial one in a sufficient energy condition. Research work [27] carried out previously has shown that interstitial atoms are able to reduce the activation energy for austenite deformation, while substitutional atoms increase the activation energy. Boron can thus move from their substitutional position to an interstitial one under hot deformation and subsequently reduce the activation energy.

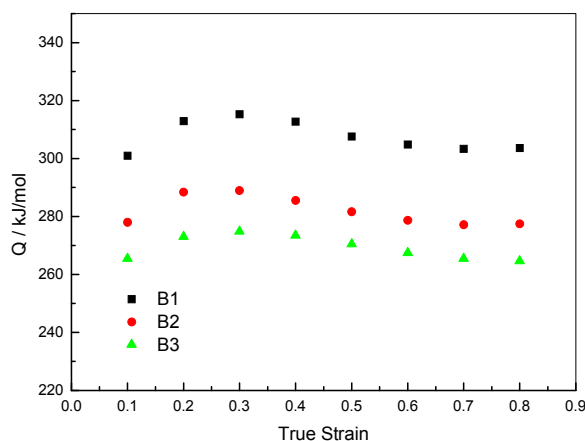


Figure 9. Effect of strain on activation energy of steels.

2.2.3. Critical DRX Parameters

To study the effect of boron content on the DRX behavior in more details, the peak stress (σ_p), critical stress (σ_c), peak strain (ε_p) and critical strain (ε_c) were analyzed according to the approach of Poliak and Jonas [28–30], an approach that is based on changes in the strain hardening rate (θ) as a function of the flow stress. In the θ - σ plot, the points at which the plot crosses the zero from above represent the peak stress, and the initiation of DRX appears as a distinct minimum in the $(-d\theta/d\sigma)$ - σ plot. Figure 10a shows the θ - σ curve for steel B2 at strain rate 0.1 s^{-1} and different temperatures. As can be seen, peak stress of steel B2 clearly increases with decreasing temperature; similarly, critical stress also clearly increases with decreasing temperature, as seen from Figure 10b. Consequently, using θ - σ and $(-d\theta/d\sigma)$ - σ curves, the peak and the critical stress and strains of tested steels can be determined for all ranges of analyzed deformation and temperature conditions.

The dependence of the characteristic points of steels under different deformation conditions on Z parameter is shown in Figure 11. It can be seen that the peak and the critical stress increase with a higher Z parameter and with the boron content. Table 3 shows the regression analysis of the curves; it can be seen that the differences of the Z parameter between the three steels is less clear.

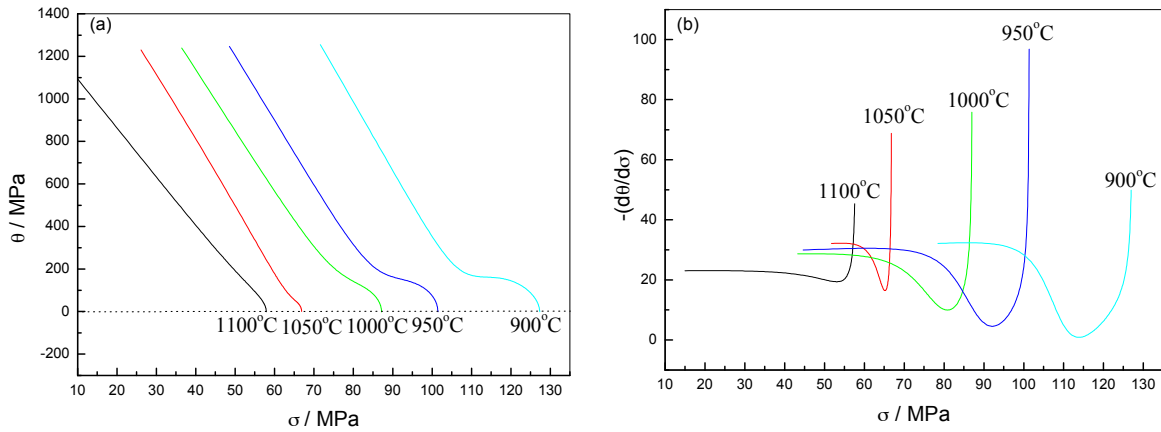


Figure 10. Strain hardening rate (θ) versus true stress at 0.1 s^{-1} for steel B2 at different temperatures. (a) θ - σ curves; (b) $-(d\theta/d\sigma)$ - σ curves.

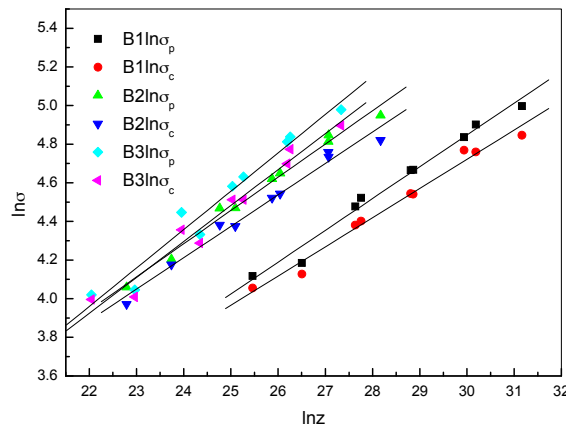


Figure 11. Relationship between σ_p , σ_c and Z for the different steels.

Table 3. The dependence of the characteristic points under different deformation conditions on Z parameter.

Steel B1		Steel B2	Steel B3
$\ln\sigma_p$ - $\ln Z$	$\ln\sigma_p = 0.16465 \ln Z - 0.09199$	$\ln\sigma_p = 0.17208 \ln Z + 0.15473$	$\ln\sigma_p = 0.19057 \ln Z - 0.40797$
$\ln\sigma_c$ - $\ln Z$	$\ln\sigma_c = 0.15116 \ln Z + 0.18716$	$\ln\sigma_c = 0.16276 \ln Z + 0.30586$	$\ln\sigma_c = 0.18593 \ln Z - 0.16590$

2.2.4. Analysis of DRX Behaviors

In Figure 12, the relationship between peak, critical stress, and the logarithms of the strain rate are plotted. As seen in the curve, peak and critical stress increase with decreasing boron content and temperature. This means that steel with higher boron content is softer than steel with lower boron content, which is in reasonable agreement with some previous reports [13–16]. It is worth mentioning that some curves show deviation from theoretical values, which is associated with experimental error and the noise level of the experimental data. Therefore, it is evident that adding boron produces softening at high temperature conditions, which is similar with respect to the role played by other elements such as carbon in steel. Recently, many investigations have reported that carbon promotes a solid solution-softening effect in steel. Sherby [31] attributed the change in creep strength to the measured increase in self-diffusivity of iron with carbon content. Wray [32] and Hai [33] confirmed

that there is a decrease in the hot flow stress when the carbon content increases. This behavior was attributed to a decrease of the work-hardening rate due to a relaxation of the austenite lattice. It has been found that flow stresses can be rationalized as a balance between work-hardening and work-softening processes. Figure 13 shows how the influence of boron content on the work-hardening rate is effective. From Figure 13, it is seen that the work-hardening rate decrease with increasing boron content at lower strain rates (0.1 and 1 s^{-1}). The results at other temperatures and lower strain rates also resemble this trend. Thus, it is inferred that the softening effect exhibited by boron increases its self-diffusivity of iron and expands austenite lattice. In addition, some researchers explained this phenomenon on the basis of the non-equilibrium segregation, as an effect of mobile vacancy-solute atom complexes diffusing through a vacancy gradient towards vacancy sinks (this gradient can be generated via plastic deformation) [13–15].

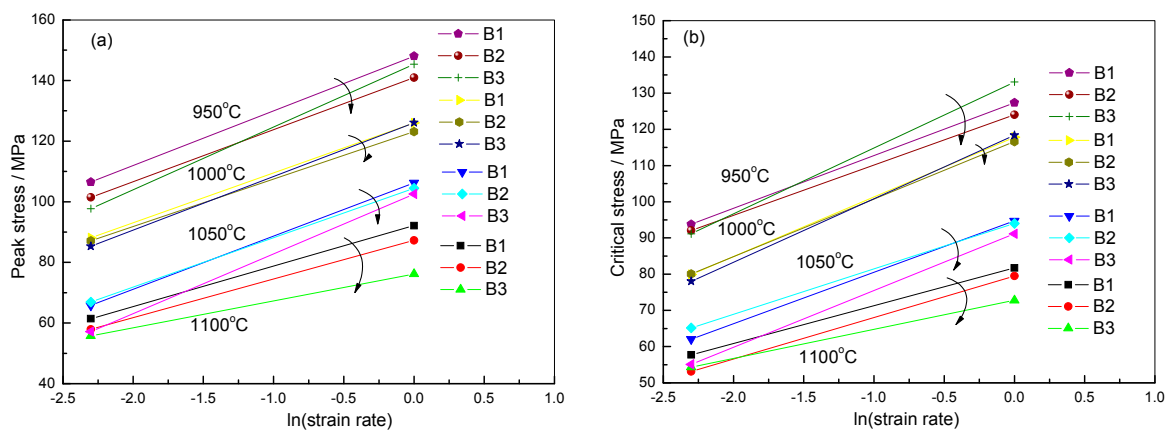


Figure 12. Relationship between peak, critical stress and the logarithm of the strain rate (a) peak stress; (b) critical stress.

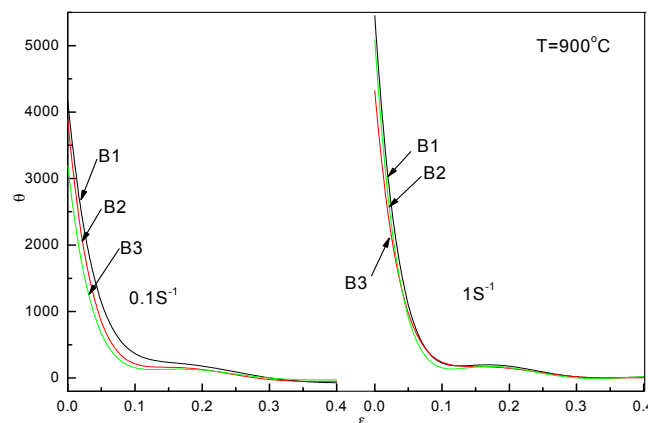


Figure 13. Strain dependence of the work-hardening rate for the experimental steels at $900 \text{ }^{\circ}\text{C}$ for strain rates of 0.1 and 1 s^{-1} .

The variation of peak and critical strain with deformation temperatures and strain rates of the experimental steels is shown in Figure 14. Some curves show deviation from theoretical values, particularly in the case of critical strain. This is associated with experimental error and fitting error. As seen in the plot, peak and critical strain increase with increasing boron content at strain rate 0.1 s^{-1} .

Therefore, the addition of boron retards the onset of DRX. These obtained results are in agreement with previous research work [16–18]. Wang [34] attributed this phenomenon to the fact that boron segregation to austenite grain boundaries retards mobility and recrystallization kinetics during hot working, which retards dynamic recrystallization when solute molecules drag by boron located on austenite grain boundaries. Moreover, the initial austenite grain size has also been shown to have an effect on the DRX behavior. The relationship between critical strain (ϵ_c) and initial austenite grain size (d_0) was found in the literature proposed by Barnett [35]. The relationship between critical strain (ϵ_c) and initial austenite grain size (d_0) was proven where the following equation was given: $\epsilon_c = 2.2 \times 10^{-4} \dot{\epsilon}^{0.24} d_0^{0.43} \exp(56500/RT)$. From this equation, critical strain is found to increase with increasing initial austenite grain size. In this case, as previously mentioned, initial austenite grain size increases with increasing boron content. It is established that, for fine grain size, the onset of DRX is promoted by the rise of the amount of available nucleation sites as the grain boundary area per unit volume is increased [36]. Therefore, the retarding onset of DRX is probably caused by the initial austenite grain size increase due to boron addition. However, it is imperative to note that peak and critical strain has a negligible change with increasing boron content at strain rate 1 s^{-1} and different temperatures except at $1100 \text{ }^\circ\text{C}$. Such behavior is attributed to the faster deformation process that does not allow for additional boron to segregate at austenite grain boundaries. Additionally, the deformation energy per time unit and the amount of available nucleation sites increase by improving strain rate. The driving force is thus significantly enhanced and becomes the primary contributing factor for the occurrence of DRX.

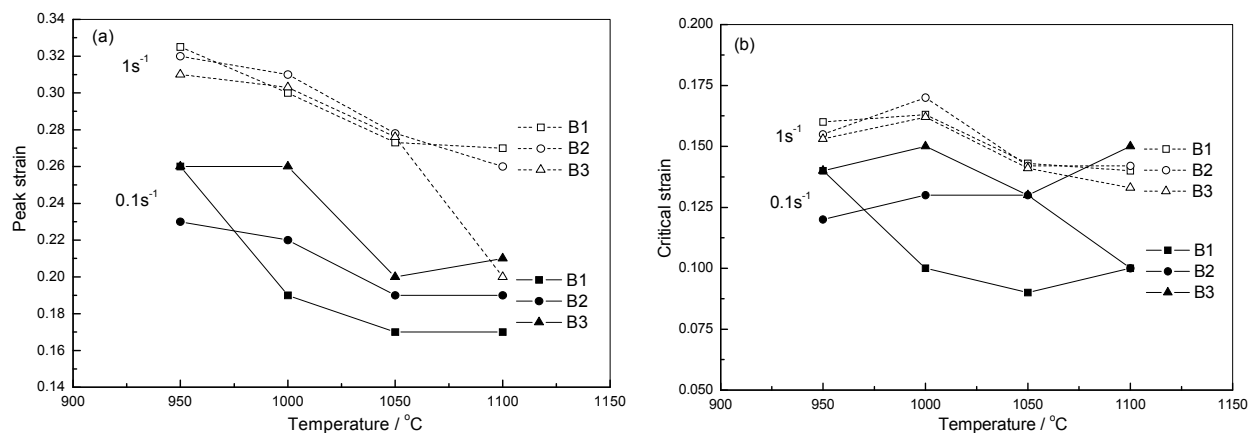


Figure 14. Peak and critical strain *versus* temperature at 0.1 and 1 s^{-1} .

3. Experimental Section

Low carbon boron-treated steels were fabricated via vacuum induction melting and the ingots were hot rolled into a 12 mm thickness plate followed by air cooling. The chemical compositions of the three steels are listed in Table 4. Cylindrical specimens 15 mm high and 8 mm in diameter were machined from the plate, and the Gleeble-2000 thermo-mechanical simulator was used for compression testing and heat treatment. For heat treatment tests, the specimens were heated to temperatures (1150, 1100 and $1050 \text{ }^\circ\text{C}$) held for 5 min, respectively, and were subsequently quenched in water immediately. In order to study the effect of boron content on hot deformation behavior,

samples were austenitized to 1150 °C at a rate of 10 °C/s and held for 180 s. Subsequently, the samples were cooled to the deformation temperature at 10 °C/s and maintained for 30 s. Five different deformation temperatures (900, 950, 1000, 1050, and 1100 °C) and three strain rates (0.1, 1, and 10 s⁻¹) were used in hot compression tests and the true strain achieved was 0.8.

Table 4. Chemical composition of the test steels (mass percent, %).

Steels	C	Si	Mn	S	P	Al	B	N
B1	0.18	0.184	0.619	0.025	0.016	0.051%	0.002	0.004
B2	0.18	0.191	0.626	0.025	0.016	0.049%	0.004	0.004
B3	0.18	0.196	0.626	0.025	0.016	0.049%	0.006	0.004

The microstructure of initial austenite grain was observed by using an optical microscope (OM) after being corroded in saturated picric acid solution. The austenite grains of 6 visual fields in every specimen were observed through the optical microscope. Each visual field was measured by the linear intercept method via image software, and the number of grains intercepted by straight lines long enough to yield at least 50 intercepts in total were counted. This ensured accuracy and utilized the mean chord length of austenite grain as a measure of its grain size. BN precipitates were observed by using scanning electron microscope (SEM) and analyzed by energy dispersive spectrometer (EDS).

4. Conclusions

(1) The initial austenite grain size of different boron content under different heating temperatures was analyzed. Results showed that the grain size in all the regions increases with an increase in the austenitization temperature, and that the austenite grain size of steel with higher boron content is larger than steel with lower boron content at each temperature. This trend can be attributed to the fact that the amount of fine AlN reduces because of the formation of BN.

(2) Increasing the boron content of boron-treated steel decreases the flow stress at lower strain rates due to the increase in self-diffusivity of iron and expansion of the austenite lattice with increasing boron content. At the same time, boron addition leads to higher flow stress at higher strain rates because of boron atoms hindering dislocation motion.

(3) The constitutive equations of hot deformation for both steels were developed. Results showed that increasing the boron content of steels has the trend to reduce the hot deformation activation energy.

(4) Increasing the boron content of boron-treated steel increases the peak and critical strain of dynamic recrystallization, indicating that boron addition can delay the onset of dynamic recrystallization.

Acknowledgments

The authors would like to acknowledge the financial support of the National Science Foundation of China (51374052), Basic Research of Key Laboratory of Education Department of Liaoning (LZ2014-022) and the Century Excellent Talent in University (NCET-11-0074).

Author Contributions

Yong-liang Gao performed the experimental work and wrote the manuscript, Xiang-xin Xue conceived and designed the study, He Yang analyzed the experiment data and assisted with the writing of the paper. All authors have read and approved the final manuscript.

Conflicts of Interest

The authors declare no conflict of interest.

References

1. Abid, N.H.; Al-Rub, R.K.A.; Palazotto, A.N. Computational modeling of the effect of equiaxed heterogeneous microstructures on strength and ductility of dual phase steels. *Comput. Mater. Sci.* **2015**, *103*, 20–37.
2. Al-Rub, R.K.A.; Ettehad, M.; Palazotto, A.N. Microstructural modeling of dual phase steel using a higher-order gradient plasticity-damage model. *Int. J. Solids Struct.* **2015**, *58*, 178–189.
3. Eghbali, B.; Abdollah-zadeh, A. Influence of deformation temperature on the ferrite grain refinement in a low carbon Nb-Ti microalloyed steel. *J. Mater. Process. Technol.* **2006**, *180*, 44–48.
4. Jun, H.J.; Kang, J.S.; Seo, D.H.; Kang, K.B.; Park, C.G. Effects of deformation and boron on microstructure and continuous cooling transformation in low carbon HSLA steels. *Mater. Sci. Eng. A* **2006**, *422*, 157–162.
5. Han, F.; Wang, B.C.; Suh, D.W.; Wang, Z.C.; Lee, D.L.; Kim, S.J. Effect of Molybdenum and Chromium on Hardenability of Low-Carbon Boron-Added Steels. *Met. Mater. Int.* **2008**, *14*, 667–672.
6. Wu, B.P.; Li, L.H.; Wu, J.T.; Wang, Z.; Wang, Y.B.; Chen, X.F.; Dong, J.X.; Li, J.T. Effect of boron addition on the microstructure and stress-rupture properties of directionally solidified superalloys. *Int. J. Miner. Metall. Mater.* **2014**, *21*, 1120–1126.
7. Chapman, M.A.V.; Faulkner, R.G. Computer modelling of grain boundary segregation. *Acta Metall.* **1982**, *31*, 677–689.
8. Nishibata, T.; Kojima, N. Effect of quenching rate on hardness and microstructure of hot-stamped steel. *J. Alloys Compd.* **2013**, *577*, S549–S557.
9. Devaa, A.; Jha, B.K.; Mishra, N.S. Influence of boron on strain hardening behavior and ductility of low carbon hot rolled steel. *Mater. Sci. Eng. A* **2011**, *528*, 7375–7380.
10. Terzic, A.; Calcagnotto, M.; Guk, S.; Schulz, T.; Kawalla, R. Influence of Boron on transformation behavior during continuous cooling of low alloyed steels. *Mater. Sci. Eng. A* **2013**, *584*, 32–40.
11. Mun, D.J.; Shin, E.J.; Choi, Y.W.; Lee, J.S.; Koo, Y.M. Effects of cooling rate, austenitizing temperature and austenite deformation on the transformation behavior of high-strength boron steel. *Mater. Sci. Eng. A* **2012**, *545*, 214–224.
12. Shigesato, G.; Fujishiro, T.; Hara, T. Grain Boundary Segregation Behavior of Boron in Low-Alloy Steel. *Metall. Mater. Trans. A* **2014**, *45*, 1876–1882.

13. Mejía, I.; Jacuinde, A.B.; Maldonado, C.; Cabrera, J.M. Determination of the critical conditions for the initiation of dynamic recrystallization in boron microalloyed steels. *Mater. Sci. Eng. A* **2011**, *528*, 4133–4140.
14. Mejía, I.; López-Chipres, E.; Maldonado, C.; Bedolla-Jacuinde, A.; Cabrera, J.M. Modeling of the hot deformation behavior of boron microalloyed steels under uniaxial hot-compression conditions. *Int. J. Mater. Res.* **2008**, *99*, 1336–1345.
15. López-Chipres, E.; Mejía, I.; Maldonado, C.; Bedolla-Jacuinde, A.; El-Wahabi, M.; Cabrera, J.M. Hot flow behavior of boron microalloyed steels. *Mater. Sci. Eng. A* **2008**, *480*, 49–55.
16. Kim, S.I.; Choi, S.H.; Lee, Y. Influence of phosphorous and boron on dynamic recrystallization and microstructures of hot-rolled interstitial free steel. *Mater. Sci. Eng. A* **2005**, *406*, 125–133.
17. Banks, K.; Stumpf, W.; Tuling, A. Inconsistent flow stress in low carbon boron steels during finishing. *Mater. Sci. Eng. A* **2006**, *421*, 307–316.
18. Stumpf, W.; Banks, K. The hot working characteristics of a boron bearing and a conventional low carbon steel. *Mater. Sci. Eng. A* **2006**, *418*, 86–94.
19. Zhang, T.; Zhang, X.M.; Guo, Z.Y.; Wang, Y.Q.; Li, C.G.; Lan, L.Y. AlN Precipitates and Microstructure in Non-oriented Electrical Steels Produced by Twin-roll Casting Process. *Acta Metall. Sin.* **2013**, *26*, 483–488.
20. Liang, Y.J.; Che, Y.C. *Thermodynamics Date of Inorganic Matter*; Northeastern University Press: Shenyang, China, 1993; p. 449.
21. Li, P.S.; Xiao, L.J.; Xie, Z. Thermodynamic Analysis of AlN and BN Competitive Precipitation in Low Carbon Steel. *J. Iron Steel Res.* **2009**, *21*, 16–18.
22. Bao, H.S.; Fu, W.T.; Cheng, S.C.; Liu, Z.D.; Yang, G. An investigation on Boronnitride (BN) Compound in T122 Heat Resistant Steel. *Iron Steel* **2005**, *40*, 68–71.
23. Chown, L.H.; Cornish, L.A. Investigation of hot ductility in Al-killed boron steels. *Mater. Sci. Eng. A* **2008**, *494*, 263–275.
24. Meysami, M.; Mousavi, S.A.A.A. Study on the behavior of medium carbon vanadium microalloyed steel by hot compression test. *Mater. Sci. Eng. A* **2011**, *528*, 3049–3055.
25. Wei, H.L.; Liu, G.Q.; Zhao, H.T.; Kang, R.M. Hot deformation behavior of two C-Mn-Si based and C-Mn-Al based microalloyed high-strength steels: A comparative study. *Mater. Des.* **2013**, *50*, 484–490.
26. Jahazi, M.; Jonas, J.J. The non-equilibrium segregation of boron on original and moving austenite grain boundaries. *Mater. Sci. Eng. A* **2002**, *335*, 49–61.
27. Stewart, G.R.; Jonas, J.J.; Montheillet, F. Kinetics and Critical Conditions for the Initiation of Dynamic Recrystallization in 304 Stainless Steel. *ISIJ Int.* **2004**, *44*, 1581–1589.
28. Poliak, E.I.; Jonas, J.J. A one-parameter approach to determining the critical conditions for the initiation of dynamic recrystallization. *Acta Mater.* **1996**, *44*, 127–136.
29. Poliak, E.I.; Jonas, J.J. Initiation of Dynamic Recrystallization in Constant Strain Rate Hot Deformation. *ISIJ Int.* **2003**, *43*, 684–691.
30. Poliak, E.I.; Jonas, J.J. Critical Strain for Dynamic Recrystallization in Variable Strain Rate Hot Deformation. *ISIJ Int.* **2003**, *43*, 692–700.
31. Sherby, O.D. Factors affecting the high temperature strength of polycrystalline solids. Factors affecting the high temperature strength of polycrystalline solids. *Acta Metall.* **1962**, *10*, 135–147.

32. Wray, P.J. Effect of carbon content on the plastic flow of plain carbon steels at elevated temperatures. *Metall. Mater. Trans. A* **1982**, *13*, 125–134.
33. Wei, H.L.; Liu, G.Q.; Zhao, H.T.; Zhang, M.H. Effect of carbon content on hot deformation behaviors of vanadium microalloyed steels. *Mater. Sci. Eng. A* **2014**, *596*, 112–120.
34. Wang, X.M.; He, X.L. Effect of Boron Addition on Structure and Properties of Low Carbon Bainitic Steels. *ISIJ Int.* **2003**, *42*, S38–S46.
35. Barnett, M.R.; Kelly, G.L.; Hodgson, P.D. Inferring dynamic recrystallization in ferrite using the kinetics of static recrystallization. *Metall. Mater. Trans. A* **2002**, *33*, 1893–1900.
36. Fernández, A.I.; Uranga, P.; López, B.; Rodríguez-Ibabe, J.M. Dynamic recrystallization behavior covering a wide austenite grain size range in Nb and Nb–Ti microalloyed steels. *Mater. Sci. Eng. A.* **2003**, *361*, 367–376.

© 2015 by the authors; licensee MDPI, Basel, Switzerland. This article is an open access article distributed under the terms and conditions of the Creative Commons Attribution license (<http://creativecommons.org/licenses/by/4.0/>).